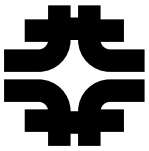

Fermi National Accelerator Laboratory

FERMILAB-Pub-97/373-E
E791

Study of the Decay $D^0 \to K^-K^+\pi^-\pi^+$

E.M. Aitala et al.
The E791 Collaboration

Fermi National Accelerator Laboratory
P.O. Box 500, Batavia, Illinois 60510

November 1997

Submitted to *Physics Letters B*

Operated by Universities Research Association Inc. under Contract No. DE-AC02-76CH03000 with the United States Department of Energy

Disclaimer

Distribution

Study of the decay $D^0 \to K^-K^+\pi^-\pi^+$

Fermilab E791 Collaboration

E. M. Aitala,[i] S. Amato,[a] J. C. Anjos,[a] J. A. Appel,[e]
D. Ashery,[o] S. Banerjee,[e] I. Bediaga,[a] G. Blaylock,[h]
S. B. Bracker,[p] P. R. Burchat,[n] R. A. Burnstein,[f] T. Carter,[e]
H. S. Carvalho,[a] N. K. Copty,[m] L. M. Cremaldi,[i] C. Darling,[s]
K. Denisenko,[e] A. Fernandez,[l] G. F. Fox,[m] P. Gagnon,[b]
C. Gobel,[a] K. Gounder,[i] A. M. Halling,[e] G. Herrera,[d]
G. Hurvits,[o] C. James,[e] P. A. Kasper,[f] S. Kwan,[e]
D. C. Langs,[k] J. Leslie,[b] B. Lundberg,[e] S. MayTal-Beck,[o]
B. Meadows,[c] J. R. T. de Mello Neto,[a] R. H. Milburn,[q]
J. M. de Miranda,[a] A. Napier,[q] A. Nguyen,[g]
A. B. d'Oliveira,[c,l] K. O'Shaughnessy,[b] K. C. Peng,[f]
L. P. Perera,[c] M. V. Purohit,[m] B. Quinn,[i] S. Radeztsky,[r]
A. Rafatian,[i] N. W. Reay,[g] J. J. Reidy,[i] A. C. dos Reis,[a]
H. A. Rubin,[f] D. A. Sanders,[i] A. K. S. Santha,[c]
A. F. S. Santoro,[a] A. J. Schwartz,[k] M. Sheaff,[d,r]
R. A. Sidwell,[g] A. J. Slaughter,[s] M. D. Sokoloff,[c] J. Solano,[a]
N. R. Stanton,[g] K. Stenson,[r] D. J. Summers,[i] S. Takach,[s]
K. Thorne,[e] A. K. Tripathi,[j] S. Watanabe,[r] R. Weiss-Babai,[o]
J. Wiener,[k] N. Witchey,[g] E. Wolin,[s] D. Yi,[i] S. Yoshida,[g]
R. Zaliznyak,[n] C. Zhang[g]

[a] *Centro Brasileiro de Pesquisas Físicas, Rio de Janeiro, Brazil*

[b] *University of California, Santa Cruz, California 95064*

[c] *University of Cincinnati, Cincinnati, Ohio 45221*

[d] *CINVESTAV, Mexico*

[e] *Fermilab, Batavia, Illinois 60510*

[f] *Illinois Institute of Technology, Chicago, Illinois 60616*

[g] *Kansas State University, Manhattan, Kansas 66506*

[h] *University of Massachusetts, Amherst, Massachusetts 01003*

[i] *University of Mississippi, University, Mississippi 38677*

[j] *The Ohio State University, Columbus, Ohio 43210*

Preprint submitted to Elsevier Preprint *4 November 1997*

[k] *Princeton University, Princeton, New Jersey 08544*
[l] *Universidad Autonoma de Puebla, Mexico*
[m] *University of South Carolina, Columbia, South Carolina 29208*
[n] *Stanford University, Stanford, California 94305*
[o] *Tel Aviv University, Tel Aviv, Israel*
[p] *317 Belsize Drive, Toronto, Canada*
[q] *Tufts University, Medford, Massachusetts 02155*
[r] *University of Wisconsin, Madison, Wisconsin 53706*
[s] *Yale University, New Haven, Connecticut 06511*

Using data from Fermilab fixed-target experiment E791, we measure the branching ratio for $D^0 \to K^-K^+\pi^-\pi^+$ and its resonant components. We find $\frac{\Gamma(D^0\to K^-K^+\pi^-\pi^+)}{\Gamma(D^0\to K^-\pi^+\pi^-\pi^+)} = (3.13 \pm 0.37 \pm 0.36)\%$. A coherent amplitude analysis is used to estimate the resonant components. We measure the ratios $\frac{\Gamma(D^0\to f)}{\Gamma(D^0\to K^-\pi^+\pi^-\pi^+)}$ to be $(2.0 \pm 0.9 \pm 0.8)\%$ for $f = \phi\rho^0$, $(0.9 \pm 0.4 \pm 0.5)\%$ for $f = \phi\pi^+\pi^-$, $< 2.0\%$ at the 90% CL for $f = K^{*0}(892)\overline{K}^{*0}(892)$, and $< 1.0\%$ at the 90% CL for $f = \overline{K}^{*0}(892)K^+\pi^-$ or $K^{*0}(892)K^-\pi^+$.

Hadronic decay mechanisms of heavy quark systems are complicated by gluon exchange processes between the initial and final states and by final-state interactions. Theoretical predictions are still limited to two-body decays, which have been analyzed extensively in the theoretical literature [1]. For example, Bauer, Stech and Wirbel [2] have used a factorization approach. Bedaqu, Das, and Mathur [3] and Kamal, Verma, and Sinha [4] have used heavy quark effective theory. More experimental data in various decay modes is essential to fully understand the decay process in heavy quark systems.

The Cabibbo-suppressed decay $D^0 \to K^-K^+\pi^-\pi^+$ [1] can be the result of intermediate two-body decays such as $D^0 \to \phi\rho^0$ and $D^0 \to \overline{K}^{*0}K^{*0}$ or it can be the result of intermediate three-body decays such as $D^0 \to \overline{K}^{*0}K^+\pi^-$. It can also occur directly as a four-body nonresonant decay. Figure 1 shows representative Feynman diagrams corresponding to each of these processes. For most intermediate states, there are two tree-level amplitudes with Cabibbo factors having opposite sign, leading to Glashow-Illiopoulos-Maiani (GIM) cancellation. Among the exceptions are $D^0 \to \phi\rho^0$ and $D^0 \to \phi\pi^+\pi^-$. The decay $D^0 \to \overline{K}^{*0}K^{*0}$ is produced from W-exchange, so it should be helicity-suppressed as well as GIM-suppressed.

[1] Throughout this paper, reference to any decay mode also implies the corresponding charge conjugate mode.

In this paper we present branching ratio and resonant substructure measurements of $D^0 \to K^-K^+\pi^-\pi^+$ made with the data from Fermilab fixed-target charm hadroproduction experiment E791. While several experimental measurements are already available on this decay mode [5-8], all previous measurements ignored the interference among the various intermediate decay amplitudes. We have used a coherent amplitude analysis, which does allow for such interference, to estimate the resonant contributions.

Experiment E791 recorded 2×10^{10} 500 GeV π^--nucleon interactions during the 1991/92 fixed-target run at Fermilab, with an open geometry spectrometer[9] in the Tagged Photon Laboratory. The segmented target consisted of one platinum foil and four diamond foils separated by gaps of 1.34 to 1.39 cm. Each foil was approximately 0.4% of an interaction length thick (0.6 mm for platinum and 1.5 mm for carbon). The average decay length of an 80 GeV D^0 is approximately 5 mm, so most of the D^0's decayed in the air gaps between target foils where backgrounds were lower. Six planes of silicon microstrip detectors (SMD) and eight proportional wire chambers (PWC) were used to track the beam particles. The downstream detector consisted of 17 planes of SMDs for vertex detection, 35 drift chamber planes, two PWCs, and two magnets for momentum analysis, two multicell threshold Čerenkov counters[10] for charged particle identification (with nominal pion thresholds of 6 GeV and 11 GeV), electromagnetic and hadronic calorimeters for electron identification and for online triggering, and two planes of muon scintillators. An interaction trigger required a beam particle and an interaction in the target. A very loose transverse energy trigger, based on the energy deposited in the calorimeters, and a fast data acquisition system [11] allowed us to collect data at a rate of 30 Mbytes/s with 50μs/event dead time and to write data to tape at a rate of 10 Mbytes/s.

Data reconstruction and additional event selection were done using offline parallel processing systems [12]. Events with evidence of well-separated production (primary) and decay (secondary) vertices were retained for further analysis. Candidate $D^0 \to K^-K^+\pi^-\pi^+$ and $D^0 \to K^-\pi^+\pi^-\pi^+$ decays were selected from events with at least one four-prong secondary vertex. Selection criteria for both modes were determined by optimizing the expected final significance of the $D^0 \to K^-K^+\pi^-\pi^+$ signal using the topologically similar $D^0 \to K^-\pi^+\pi^-\pi^+$ signal and assuming the $K^-K^+\pi^-\pi^+$ signal would be about sixty times smaller. The decay vertex was required to be well-separated from the primary vertex with $\Delta z \ > \ 8\,\sigma_z$ where σ_z is the error on Δz, the separation between two vertices. The vertex was required to lie outside the target foils and other solid material with $\Delta t \ > \ 4.5\,\sigma_t$, where σ_t is the error on Δt, the distance to the closest solid material. The momentum vector of the candidate D^0 was required to point back to the primary vertex with transverse miss distance less than 45 μm, and the tracks emerging from the secondary vertex were required to miss the primary vertex with normalized impact pa-

rameters greater than $4\sigma_d$ where σ_d is the error on the separation between the track and the primary vertex. In addition, kaon signatures were required in the Čerenkov detector system which provided kaon identification in the range 6 - 60 GeV. To simplify normalization, only pion and kaon candidates in that momentum range were used.

Branching Ratio Measurement

The signal level in each mode was estimated using unbinned maximum likelihood fits to the observed invariant-mass distributions assuming Gaussian signal and linear background shapes. Figure 2 shows the final observed $K^-K^+\pi^-\pi^+$ and $K^-\pi^+\pi^-\pi^+$ mass spectra with the best fits superimposed. The fits found 136 ± 15 $D^0 \to K^-K^+\pi^-\pi^+$ and 8245 ± 101 $D^0 \to K^-\pi^+\pi^-\pi^+$ signal events. Although the track and vertex selection criteria for the two decay modes were identical, the geometric acceptances and reconstruction efficiencies differed because of the different kinematics and resonant substructures of the decay modes. Monte Carlo (MC) events based on the PYTHIA and JETSET event generators [13] and a detailed E791 spectrometer simulation were used to study these effects. Considering all factors other than Čerenkov identification of kaons, and using nonresonant MC events, the acceptance for $K^-K^+\pi^-\pi^+$ relative to $K^-\pi^+\pi^-\pi^+$ was determined to be 91%. This value varied by about $\pm 5\%$ when MC events with different resonant substructures were used. The detection efficiencies for the two modes also differ because the $K^-K^+\pi^-\pi^+$ decay has two kaons which require Čerenkov identification whereas the $K^-\pi^+\pi^-\pi^+$ decay has only one. The efficiency of the Čerenkov selection criteria used to identify kaons was estimated by comparing $D^0 \to K^-\pi^+\pi^-\pi^+$ signals with and without the Čerenkov selection criteria. For the Čerenkov requirement used in this analysis, the efficiency for kaon identification was found to be $(59 \pm 6)\%$. This algorithm for determining the relative Čerenkov efficiencies was validated using MC data, although we did not use absolute Čerenkov efficiencies in this analysis. MC events were also used to study possible feedthrough to the signal from misidentified charm decays such as $D^0 \to K^-\pi^+\pi^-\pi^+\pi^0$. We did not find any significant feedthrough to the $D^0 \to K^-K^+\pi^-\pi^+$ signal after the final selection criteria.

Sources of systematic uncertainties include the detector simulation, the background shapes, acceptance and efficiency dependencies on resonant components, and the relative efficiency for Čerenkov particle identification for the two decay modes. The total fractional systematic uncertainty was estimated to be 12% and was dominated by the fractional uncertainty in the Čerenkov efficiency (10%).

With these relative acceptances and efficiencies, we measured the ratio of

decay widths to be

$$\frac{, (D^0 \to K^- K^+ \pi^- \pi^+)}{, (D^0 \to K^- \pi^+ \pi^- \pi^+)} = (3.13 \pm 0.37 \pm 0.36)\%. \quad (1)$$

Using the $D^0 \to K^- \pi^+ \pi^- \pi^+$ branching fraction reported in the Review of Particle Physics [14], 7.5 ± 0.4 %, and folding its error into our final systematic error, we obtain

$$B(D^0 \to K^- K^+ \pi^- \pi^+) = (0.254 \pm 0.030 \pm 0.033)\%. \quad (2)$$

Resonant Substructure Measurement

The resonant substructure of the decay $D^0 \to K^- K^+ \pi^- \pi^+$ was studied using events from the branching fraction sample with 1835 MeV $< m(KK\pi\pi) <$ 1895 MeV (the shaded region in the upper histogram of Fig. 2). Contributions from resonant modes to the observed signal were estimated using a series of maximum likelihood fits. We included some or all of the intermediate resonant states listed in Table 1 in each of our candidate descriptions of the data. For each model of the data, we performed a coherent amplitude analysis to extract relative magnitudes and phases of amplitudes. From these, we extracted decay fractions for each mode and for several combinations of modes. We compared the results of fits with different combinations of amplitudes to determine which were significant and to estimate relevant systematic uncertainties. The technique used is similar to amplitude analyses performed by other experiments in various three- and four-body decays [15]. For each fit we maximized a likelihood function $\mathcal{L}$ which had the form

$$\mathcal{L} = \frac{e^{-\nu} \nu^n}{n!} \prod_{j=1}^{n} \mathcal{P}_j \quad (3)$$

where n is the number of events in the data sample, ν is the number of events estimated by the fit, and $\mathcal{P}_j$ is the probability of the j^{th} event occurring. It is given by

$$\mathcal{P}_j = \frac{S \cdot \mathcal{P}_{jS} + B \cdot \mathcal{P}_{jB}}{S + B}. \quad (4)$$

where S and B are the numbers of signal and background events determined by the fit such that

$$\nu = S + B. \quad (5)$$

The probability density function for the signal has the form

$$\mathcal{P}_{jS} = \frac{1}{\sqrt{2\pi}\sigma} \exp\left(\frac{-(M_j - M_0)^2}{2\sigma^2}\right) \frac{1}{N_S} \epsilon_j \left| \sum_{k=1}^{m} A_k \mathcal{M}_k^S(x_j) e^{i\alpha_k} \right|^2 . \qquad (6)$$

Here, M_0 and σ are the fitted mean and width of the D^0 signal observed in the $K^-K^+\pi^-\pi^+$ invariant mass distribution, and M_j and ϵ_j are the $K^-K^+\pi^-\pi^+$ invariant mass and expected efficiency for the j^{th} event. The Gaussian factor accounts for the observed D^0 mass resolution and the sums are taken over nonresonant and resonant amplitudes used in the fit. N_S is a normalization factor. A_k and α_k are the magnitude and phase of the k^{th} contributing amplitude, and $\mathcal{M}_k^S(x_j)$ is the corresponding matrix element calculated for the kinematic variables x_j which describe the location of the j^{th} event in four-body phase space. For the nonresonant mode, $\mathcal{M}_k^S(x_j)$ was taken to be a constant. For modes containing resonances, $\mathcal{M}_k^S(x_j)$ is represented by a product of relativistic Breit-Wigner functions for the resonances in the mode [16]

$$\mathcal{M}_k^S(x_j) = N_k^S \prod_i \frac{1}{m_{i,j}^2 - m_{0i}^2 + i m_{0i},\ {}_{0i}}; \qquad (7)$$

m_{0i} and , ${}_{0i}$ are the mass and width of resonance i and $m_{i,j}$ is the invariant mass for resonance i calculated for event j. N_k^S is a normalization factor such that the integral of $\mathcal{M}_k^S(x_j)$ over phase space is unity. Because there are many possible intermediate states with various spins that cannot be resolved with our limited statistics, we do not include angular distributions, momentum dependent partial widths, or form factors in the matrix elements.

The background allowed in the fit consists of a component uniform in four-body phase space and components containing ϕ, $K^{*0}(892)$, $\overline{K}^{*0}(892)$, and ρ^0 resonances, and the K_S^0. The probability density function for the background has the form

$$\mathcal{P}_{jB} = (C + s(M_j - M_0)) \frac{1}{N_B} \sum_k \epsilon_j b_k |\mathcal{M}_k^B(x_j)|^2 \qquad (8)$$

which is linear in the $K^-K^+\pi^-\pi^+$ invariant mass M_j and includes uniform and resonant backgrounds. N_B is the normalization factor for the sum over all modes; s is the slope of the distribution; C is a constant term chosen to give unit normalization to $\mathcal{P}_{jB}$ over the mass window used in the fit; b_k is the relative fraction of each background; and $\mathcal{M}_k^B(x_j)$ is the corresponding background matrix element. For the uniform background, $\mathcal{M}_k^B$ is taken to be a constant and for the resonances the following form of Breit-Wigner function

was used:

$$\mathcal{M}_k^B(x_j) = \frac{N_k^B}{m_{k,j}^2 - m_{0k}^2 + im_{0k,\ 0k}}; \tag{9}$$

N_k^B is a normalization constant such that the integral of $\mathcal{M}_k^B(x_j)$ over phase space is unity. The background probability density function is a sum over probabilities rather than the square of a sum over amplitudes because the sources of background should add incoherently.

Nonresonant $K^-K^+\pi^-\pi^+$ Monte Carlo events (which uniformly populate four-body phase space) were used to numerically calculate the normalizations N_S, N_B, N_k^S, and N_k^B, and other integrals which appear in intermediate stages of the likelihood fit. We implicitly account for geometric acceptance and reconstruction efficiency by using reconstructed Monte Carlo events that passed successfully through the analysis selection criteria to calculate all such integrals. Therefore, no separate calculations of these effects are needed.

The parameters of the fit are relative rather than absolute amplitudes (magnitudes A_k and phases α_k). Were all the magnitudes scaled by the same constant, or were the same constant added to all the phases, the physics (the fit fractions and relative phases) would remain the same. Therefore, one signal matrix element (its magnitude and phase) was fixed for each fit. The decay fractions were calculated by integrating the signal intensity (which is proportional to the square of the amplitude or coherent sum of amplitudes, depending on whether the mode is a single decay or a combination of decays) for that mode alone divided by the integrated intensity with all modes present. Integration was done numerically using the same MC event sample used to calculate normalizations.

Likelihood maximization was done with MINUIT [17]. Because there was a clear indication of significant $D^0 \to \phi\rho^0$ signal in the data, amplitudes (magnitudes and phases) of other contributing modes were measured relative to the $D^0 \to \phi\rho^0$ amplitude. All fits were done with the events in the mass window $|M(K^-K^+\pi^-\pi^+) - 1865\ \text{MeV}| < 30\ \text{MeV}$ (the shaded region in the upper histogram of Fig. 2). Because this selection did not provide enough side-band events to make a good estimate of the background level, the background slope s and the height C of Eq. (8) were fixed at the values obtained from the fit used to extract the branching fraction (shown in Figure 2). We tried many fits with various combinations of the intermediate states listed in Table 1. To ensure that each fit converged to a true maximum, not to a local maximum, we repeated each fit at least five times with substantially different initial values for all the parameters.

Because $K_1^+(1400) \to \overline{K}^{*0}(892)\pi^+$, the decays $D^0 \to K^{*0}(892)K^-\pi^+$ and

$D^0 \to K_1^+(1400)K^-$ have almost identical two- and three-body invariant mass distributions except for the broad Breit-Wigner distribution of $K_1^+(1400)$. Fits which included both of these amplitudes did not improve the likelihood significantly. Rather, the amplitudes for each of these two amplitudes became large, highly uncertain, and interfered destructively. Therefore, we did not allow $K_1^+(1400)$ in the final fit, and we kept only the mode $D^0 \to K^{*0}(892)K^-\pi^+$.

Because we did not have enough events to separate D^0 from $\overline{D}^0$ (*e.g.*, through the decay $D^{*+} \to D^0\pi^+$), we could not distinguish $D^0 \to K^{*0}(892)K^-\pi^+$ from $\overline{D}^0 \to K^{*0}(892)K^-\pi^+$. Thus, we report an upper limit for D^0 decaying to the sum of $K^{*0}(892)K^-\pi^+$ and $\overline{K}^{*0}(892)K^+\pi^-$ modes.

Because $K_1^-(1270) \to \rho^0 K^-$, the decays $D^0 \to K_1^-(1270)K^+$ and $D^0 \to \rho^0 K^- K^+$ produce two- and three-body invariant mass distributions which are indistinguishable, given the number of events used in the fit. They are also very similar to the distributions for nonresonant decays. Of these three modes, we used only the nonresonant and the $D^0 \to \rho^0 K^- K^+$ amplitudes in our fit.

The fit whose results we report included amplitudes for modes 1-7 of Table 1 for the signal, and for background allowed a component uniform in four-body phase space and components containing ϕ, $K^{*0}(892)$, $\overline{K}^{*0}(892)$, and ρ^0 resonances, and the K_S^0. Its projections on various two and three-body invariant mass distributions had good values of chi-square per degree of freedom. Figure 3 shows these projections of the data and of the reported fit for various two- and three-body invariant mass distributions for events in the signal region ($|M(K^-K^+\pi^-\pi^+) - 1865\,\mathrm{MeV}| < 12$ MeV) and in the background regions (12 MeV $< |M(K^-K^+\pi^-\pi^+) - 1865\,\mathrm{MeV}| < 30$ MeV). The maximum vertical scales for the background region plots are 50% greater than those for the signal region plots because the background region used in the fit was 50% wider than the signal region used in the fit. The values of chi-square per degree of freedom shown in the plots were calculated for each projection using the errors on the observed numbers of events to normalize the differences between the observed and projected numbers of events and using the number of bins with data entries as the number of degrees of freedom. Much of the apparent structure in these two- and three-body invariant mass plots can be the result of resonant structure in other variables. For example, the accumulation of events at large $K\pi\pi$ invariant mass is a feature expected in $D^0 \to \overline{K}^* K^*$ and $D^0 \to \phi\pi\pi$; it does not require the presence of an excited K state.

The decay fractions for the modes in the fit are reported in Table 2. The systematic errors include uncertainties due to exclusion of some amplitudes from the fit (which are the dominant contributions), Monte Carlo statistical errors, and the uncertainties in the resonance widths and masses. To test the sensitivity of our results to ignoring form factors and momentum factors in the matrix elements describing amplitudes with K^{*0} and ϕ resonances, the

K^{*0} and ϕ signals from $D_S^+ \to K^+K^-\pi^+$ and $D^+ \to K^+K^-\pi^+$ were fit with and without those factors. The differences were negligible. The ability of the fit to correctly extract magnitudes and phases of amplitudes was confirmed using Monte Carlo studies.

Table 3 shows decay rates for several modes relative to that for $D^0 \to K^-\pi^+\pi^-\pi^+$ and compares them to measurements from other experiments. Because the intermediate resonances can have decay modes in addition to those we observed, these D^0 relative decay rates have been corrected for the exclusive branching ratios of the intermediate resonances using Particle Data Group[14] values. Table 4 compares our measured branching fractions for $D^0 \to \phi\rho^0$ and $D^0 \to \overline{K}^{*0}K^{*0}$ to theoretical predictions.

The analysis in this letter is the first reported to allow interference among amplitudes in the decay $D^0 \to K^-K^+\pi^-\pi^+$. The significant phase angles among different modes reported in Table 2 indicate that such interference is very strong. As a consequence of the additional variation allowed in this analysis, the errors on decay fractions are larger than those reported by other experiments.

Conclusions

In conclusion, we have measured , $(D^0 \to K^-K^+\pi^-\pi^+)/$, $(D^0 \to K^-\pi^+\pi^-\pi^+)$ to be $(3.13 \pm 0.37 \pm 0.36)\%$, somewhat lower than the naive expectation of $\tan^2\theta_C = 5\%$. This may be evidence of the tree-level GIM suppression expected for most of the amplitudes. Our analysis of the resonant substructure of $D^0 \to K^-K^+\pi^-\pi^+$ decays reveals a substantial fraction of decays into $\phi\pi^+\pi^-$ (nonresonant) and/or $\phi\rho^0$ (see Table 2); these modes are not GIM suppressed at tree-level. Due to limited statistics and interference effects, we obtained only upper limits for the decay mode $D^0 \to K^{*0}\overline{K}^{*0}$, and for the sum of the modes $D^0 \to K^{*0}K^-\pi^+$ and $D^0 \to \overline{K}^{*0}K^+\pi^-$. Our results for $D^0 \to \phi\rho^0$ and $D^0 \to K^{*0}\overline{K}^{*0}$ are consistent with theoretical predictions and other experimental measurements.

Acknowledgement

We gratefully acknowledge the assistance of the staffs of Fermilab and of all the participating institutions. This research was supported by the Brazilian Conselho Nacional de Desenvolvimento Científico e Tecnológico, CONACYT (Mexico), the U.S.-Israel Binational Science Foundation, and the U.S. National Science Foundation. Fermilab is operated by the Universities Research Associates, Inc., under contract with the United States Department of Energy.

References

[1] I.I. Bigi, in: Proceedings of CCAST Symposium. Vol. 2 Charm Physics, eds. Ming-han Ye and Tao Huang, Gordon and Breach (1987) 339; M. Wise, in: Proceedings of the International Symposium on Heavy Flavour Physics, Montreal 1993, Editions Frontieres (1994) 5; R. S. Orr, in: *Proceedings of Heavy Flavor Decay and Mixing* in Selected Topics in Electroweak Interactions, ed. J. M. Cameron, World Scientific (1987) 1.

[2] M. Bauer, B. Stech and M. Wirbel, Z. Phy. 34 (1987) 103.

[3] P. Bedaqu, A. Das and V.S. Mathur, Phys. Rev. D 49 (1994) 269.

[4] A.N. Kamal, R.C. Verma and N. Sinha, Phys. Rev. D 43 (1991) 843.

[5] E691 Collaboration, J.C. Anjos *et al.*, Phys. Rev. D 43 (1991) 6351.

[6] CLEO Collaboration, R. Ammar *et al.*, Phys. Rev. D 44 (1991) 3383.

[7] ARGUS Collaboration, H. Albrecht *et al.*, Z. Phys. C 64 (1994) 375.

[8] E687 Collaboration, L. Frabetti *et al.*, Phys. Lett. B 354 (1995) 486.

[9] J.A. Appel, Ann. Rev. Nucl. Part. Sci. **42**, (1992) 367, and references therein; D.J. Summers *et al.*, in: Proceedings of the *XXVII* $^{\text{th}}$ *Rencontre de Moriond*, Electroweak Interactions and Unified Theories, Les Arc, France (15-22 March, 1992) 417.

[10] D. Bartlett *et al.*, Nucl. Instr. and Meth. A 260 (1986) 55.

[11] S. Amato *et al.*, Nucl. Instr. and Meth. A 324 (1993) 535.

[12] F. Rinaldo and S. Wolbers, Computers in Physics 7 (1993) 184; S. Bracker *et al.*, IEEE Trans. Nucl. Sci. 43 (1996) 2457.

[13] PYTHIA 5.7 and JETSET 7.4 Physics Manual, CERN-TH-7112/93 (1993).

[14] Review of Particle Physics, R. M. Barnett *et al.*, Phys. Rev. D 54 (1996) 455.

[15] ARGUS Collaboration, H. Albrecht *et al.*, Phys. Lett. B 308 (1993) 435; E687 Collaboration, P.L. Frabetti *et al.*, Phys. Lett. B 331 (1994) 217; MARK III Collaboration, D. Coffman *et al.*, Phys. Rev D 45 (1992) 2196.

[16] J. D. Jackson, Nuovo Cimento Vol. $XXXIV$, N6 (1964) 1645.

[17] MINUIT Reference Manual, CERN Program Library Long Writeup, PM0020 (1994).

Table 1
Intermediate modes of $D^0 \to K^-K^+\pi^-\pi^+$ and resonant decay modes considered in the fit. Only modes 1 through 7 were used in the reported fit.

1	$D^0 \to K^-K^+\pi^+\pi^-$ nonresonant
2	$D^0 \to \overline{K}^{*0}(892)K^{*0}(892)$, $\overline{K}^{*0}(892) \to K^-\pi^+$, $K^{*0}(892) \to K^+\pi^-$
3	$D^0 \to K^{*0}(892)K^-\pi^+$, $K^{*0}(892) \to K^+\pi^-$
4	$D^0 \to \overline{K}^{*0}(892)K^+\pi^-$, $\overline{K}^{*0}(892) \to K^-\pi^+$
5	$D^0 \to \phi\rho^0$, $\phi \to K^+K^-$, $\rho^0 \to \pi^+\pi^-$
6	$D^0 \to \phi\pi^+\pi^-$, $\phi \to K^+K^-$
7	$D^0 \to \rho^0K^+K^-$, $\rho^0 \to \pi^+\pi^-$
8	$D^0 \to K_1^-(1270)K^+$, $K_1^-(1270) \to K^-\rho^0$, $\rho^0 \to \pi^+\pi^-$
9	$D^0 \to K_1^+(1270)K^-$, $K_1^+(1270) \to K^+\rho^0$, $\rho^0 \to \pi^+\pi^-$
10	$D^0 \to K^-(1400)K^+$, $K^-(1400) \to \overline{K}^{*0}(892)\pi^-$, $\overline{K}^{*0}(892) \to K^-\pi^+$
11	$D^0 \to K^+(1400)K^-$, $K^+(1400) \to K^{*0}(892)\pi^+$, $K^{*0}(892) \to K^+\pi^-$

Table 2
Final fit results for the decay fractions to $D^0 \to K^-K^+\pi^-\pi^+$. The decay fractions for single amplitudes or combinations of amplitudes are calculated as described in the text. The phases for single amplitudes are those extracted from the fit relative to that for $D^0 \to \phi\rho^0$.

Decay mode	Decay Fractions	relative phase angle
$D^0 \to \phi\rho^0$	$0.21 \pm 0.10 \pm 0.08$	0
$D^0 \to \phi\pi^+\pi^-$	$0.14 \pm 0.06 \pm 0.04$	$(180 \pm 19 \pm 6)^\circ$
$D^0 \to \phi\rho^0 + \phi\pi^+\pi^-$	$0.18 \pm 0.05 \pm 0.06$	
$D^0 \to \overline{K}^{*0}K^{*0}$	$0.13 \pm 0.10 \pm 0.06$	$(76 \pm 28 \pm 6)^\circ$
$D^0 \to \overline{K}^{*0}K^+\pi^- + K^{*0}K^-\pi^+$	$0.04 \pm 0.11 \pm 0.14$	
$D^0 \to K^-K^+\pi^-\pi^+$ nonresonant	$0.7 \pm 0.6 \pm 0.3$	$(97 \pm 12 \pm 10)^\circ$
$D^0 \to \rho^0K^-K^+$	$0.6 \pm 0.5 \pm 0.3$	$(-88 \pm 13 \pm 12)^\circ$
$D^0 \to K^-K^+\pi^-\pi^+$ nonresonant		
$+ \rho^0K^-K^+$	$0.5 \pm 0.8 \pm 0.4$	

Table 3
E791 $D^0 \to K^-K^+\pi^-\pi^+$ decay rate measurements, relative to $D^0 \to K^-\pi^+\pi^-\pi^+$, compared to those of other experiments. Only E791 has accounted for interference between amplitudes. Values reported here have been corrected for exclusive branching ratios of the subresonances using PDG values[14]. All upper limits are at the 90% confidence level.

Decay mode (f)	, $(D^0 \to f) \times 100$ / , $(D^0 \to K^-\pi^+\pi^-\pi^+)$				
	E791	E691[5] (1991)	CLEO[6] (1991)	ARGUS[7] (1994)	E687[8] (1995)
inclusive $K^-K^+\pi^-\pi^+$	$3.13 \pm 0.37 \pm 0.36$	$2.8^{+0.8}_{-0.7}$	3.14 ± 1.0	$4.1 \pm 0.7 \pm 0.5$	$3.4 \pm 0.4 \pm 0.4$
$D^0 \to \phi\rho^0$	$2.0 \pm 0.9 \pm 0.8$		2.4 ± 0.6	$2.0 \pm 0.6 \pm 0.5$	0.5 ± 0.3
$D^0 \to \phi\pi^+\pi^-$	$0.9 \pm 0.4 \pm 0.5$	$0.76^{+0.66}_{-0.49}$			< 0.6
$D^0 \to K^{*0}\overline{K}^{*0}$	< 2.0	$3.6^{+2.0}_{-1.6}$	< 3.3		1.6 ± 0.6
$D^0 \to K^{*0}K^-\pi^+$	< 1.0	$1.0^{+1.6}_{-1.0}$		$4.3 \pm 1.4 \pm 0.9$	< 1.7
$+ \overline{K}^{*0}K^+\pi^-$				$2.3 \pm 1.3 \pm 0.9$	

Table 4
E791 measured branching fractions compared to theoretical predictions.

Decay	B($D^0 \to \phi\rho^0$)	B($D^0 \to \overline{K}^{*0}K^{*0}$)
E791	$(1.6 \pm 0.5 \pm 0.5) \times 10^{-3}$	$< 1.6 \times 10^{-3}$
BSW [2]	$(1.0 \pm 0.3) \times 10^{-3}$	
BDM[3]	2.2×10^{-4}	2.6×10^{-5}
KVS[4]	(2.6 - 8.0) $\times 10^{-4}$	

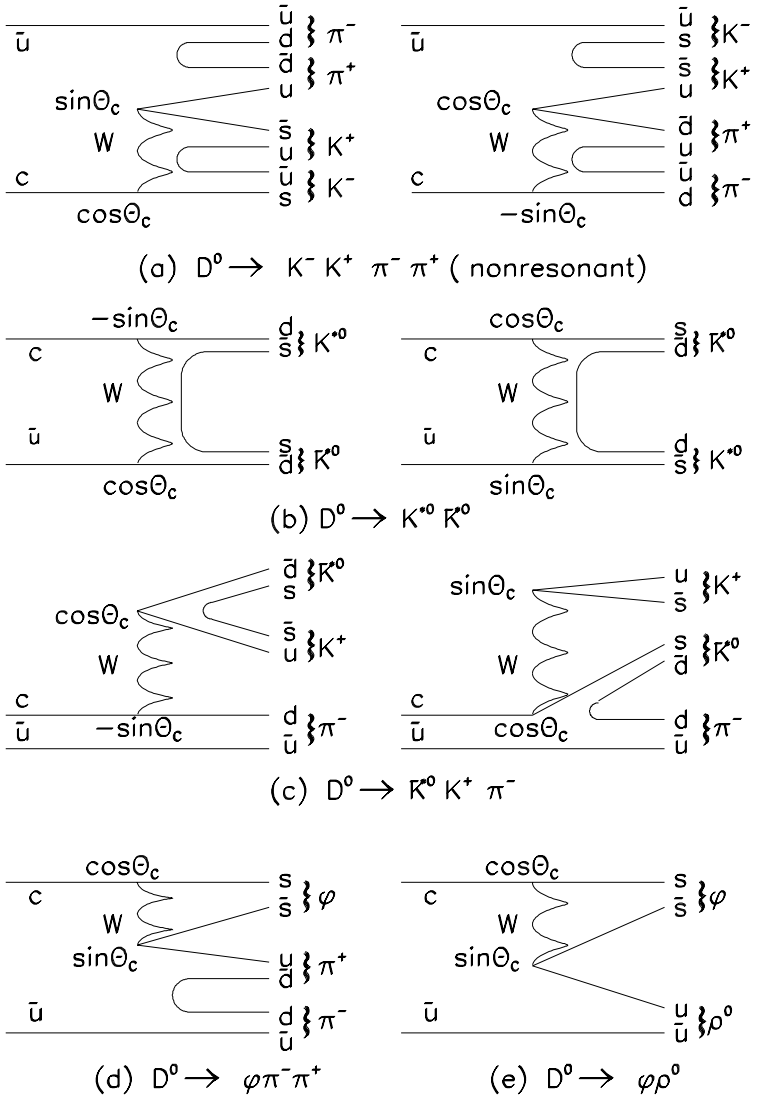

Fig. 1. Representative Feynman diagrams for some of the modes which might contribute to $D^0 \to K^-K^+\pi^-\pi^+$.

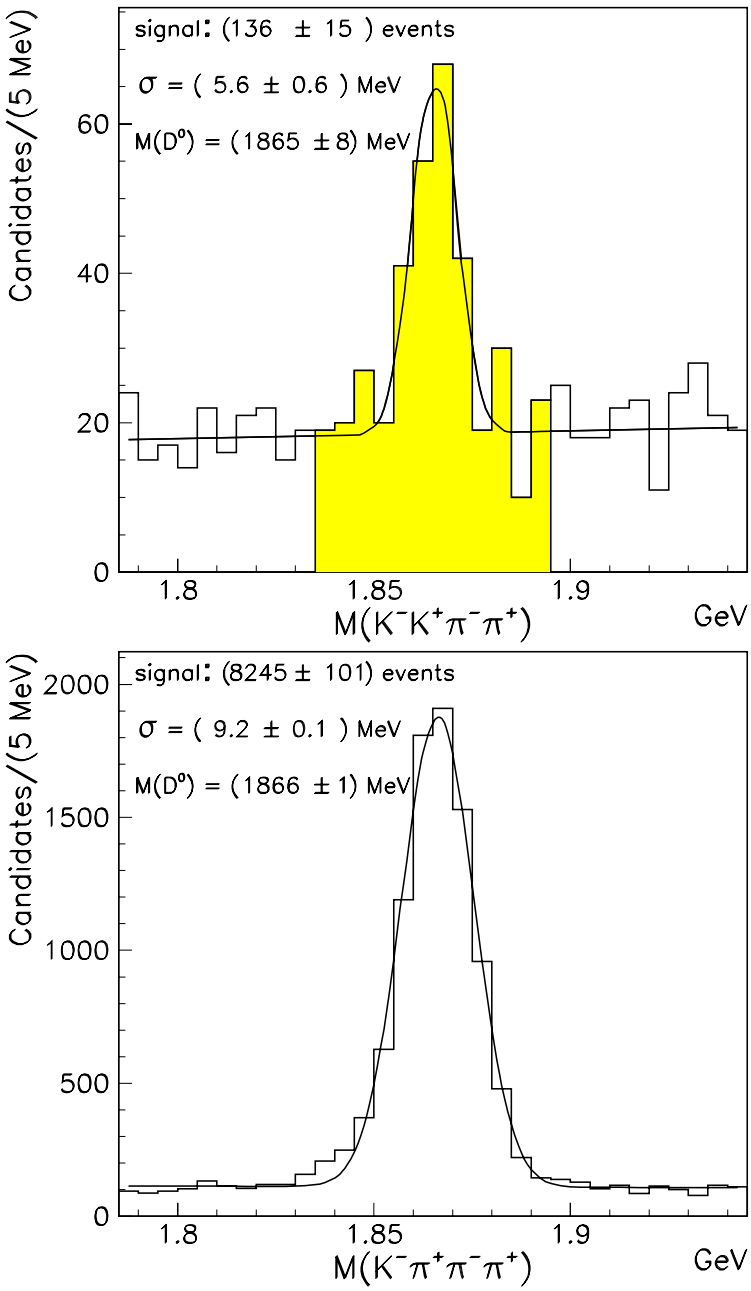

Fig. 2. Invariant masses of $D^0 \to K^-K^+\pi^-\pi^+$ and $D^0 \to K^-\pi^+\pi^-\pi^+$ candidates after the final selection criteria with the branching fraction measurement fits superimposed. The events in the shaded region of the top histogram were used in the resonant substructure analysis.

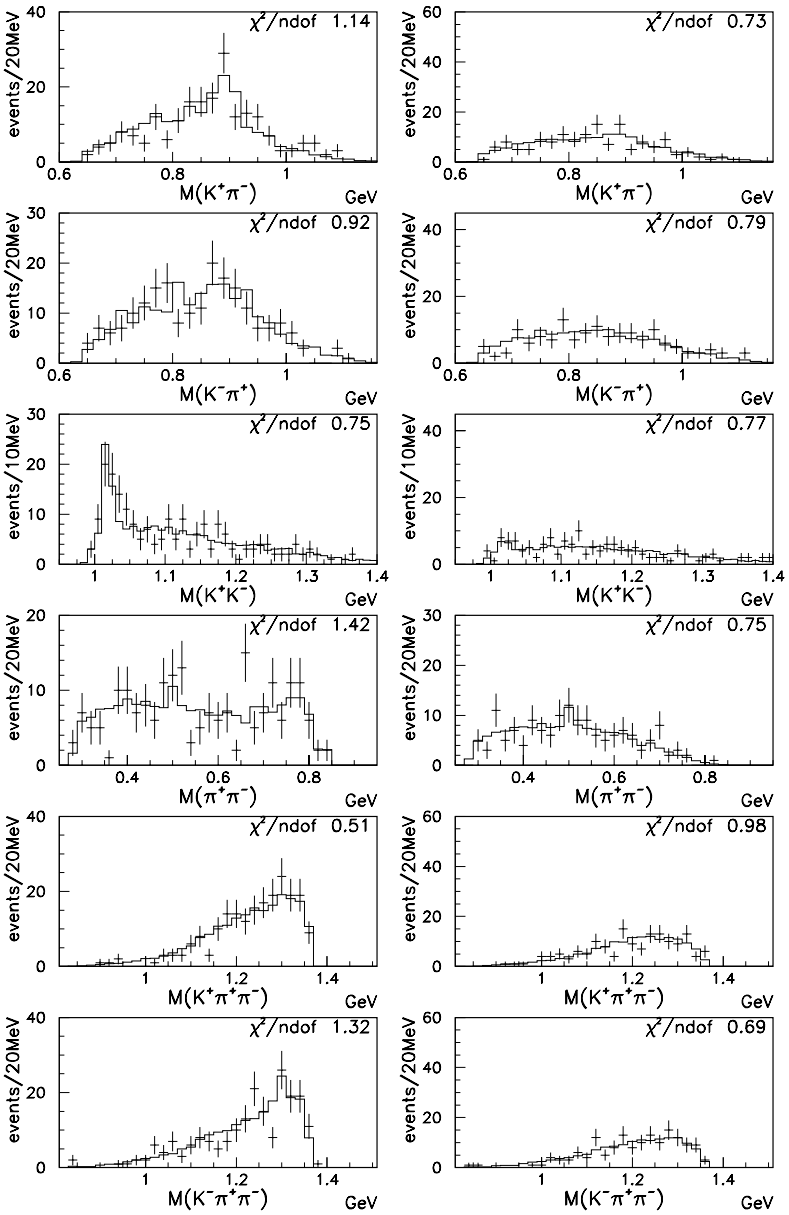

Fig. 3. Projections of the data and the fit, for events in the signal region ($|M(K^-K^+\pi^-\pi^+) - 1865$ MeV $| < 12$ MeV) (left) and for the background region (12 MeV $< |M(K^-K^+\pi^-\pi^+) - 1865$ MeV $| < 30$ MeV) (right). The data are indicated by points with error bars and the fit projections by the histograms. Amplitudes for modes 1 through 7 of Table 1 were used to describe the signal while amplitudes for uniform phase space and amplitudes containing K^{*0}, $\overline{K}^{*0}$, ρ^0, ϕ, and K_s resonances were used to describe the background. See the text for further discussion of scales and chi-square values.